Measured oscillations of the velocity and temperature fields in turbulent Rayleigh-Bénard convection in a rectangular cell

Sheng-Qi Zhou,* Chao Sun, and Ke-Qing Xia
Department of Physics, The Chinese University of Hong Kong, Satin, Hong Kong, China
(Received 3 May 2007; published 10 September 2007)

Temperature and velocity oscillations have been found in a rectangular Rayleigh-Bénard convection cell, in which one large-scale convection roll exists. At Rayleigh number $\mathrm{Ra}=8.9\times10^{11}$ and Prandtl number $\mathrm{Pr}=4$, temperature oscillations can be observed in most parts of the system and the oscillation period remains almost constant, $t_T=74\pm2$ s. Velocity oscillation can only be found in its horizontal component v_y (perpendicular to the large-scale circulation plane) near the cell sidewall, its oscillation period is also constant, $t_v=65\pm2$ s, at these positions. Temperature and velocity oscillations have different Ra dependences, which are, respectively, indicated by the Péclect number $\mathrm{Pe}_T=0.55\mathrm{Ra}^{0.47}$ and $\mathrm{Pe}_v=0.28\mathrm{Ra}^{0.50}$. In comparison to the case of a cylindrical cell, we find that velocity oscillations are affected by the system geometry.

DOI: 10.1103/PhysRevE.76.036301 PACS number(s): 47.27.te, 05.65.+b, 44.25.+f

I. INTRODUCTION

The coherent large-scale flow structure is one of the most important constituents in turbulent thermal convections, which occur widely in the oceans, the atmosphere, Earth's outer core, and galaxies [1]. Its detailed flow dynamics has been mainly investigated in the classical Rayleigh-Bénard convection system, where a confined enclosure is heated from below and cooled from above [2–4]. The system has three control parameters: namely, the Rayleigh number (Ra), Prandtl number (Pr), and aspect ratio (Γ). The Rayleigh number is defined as $\mathrm{Ra}=\alpha g L^3\Delta T/\nu\kappa$, with g being the gravitational acceleration, and α, ν, and κ being, respectively, the thermal expansion coefficient, the kinematic viscosity, and the thermal diffusivity of working fluid. The Prandtl number is defined as $\mathrm{Pr}=\nu/\kappa$, and the aspect ratio Γ is the ratio of the lateral dimension of the system to its height. In the system, a prominent self-sustained low-frequency oscillation of the measured local velocity and/or temperature has been generally observed in numerous experiments and numerical simulations [3–28]. However, the origin of this characteristic frequency still remains elusive, although much effort has been made to tackle this issue in the past decades.

Explanation of low-frequency oscillations can be traced to the "bubble model" [3] and later the "plume model" [14], which were developed based on the presence and persistence of thermal structures (e.g., thermals, plumes) [2]. It is assumed that a thermal boundary layer thickens in time by the upward diffusion of the temperature field. When a critical thickness is attained, the boundary layer will erupt and quickly expel all buoyant fluid through plumes and thermals away from the boundary. The depleted boundary layer thus grows once more by diffusion, and the process repeats in a periodic manner. Such a phenomenological picture has been observed in high-Pr fluid with the shadowgraph technique [29]. In later experiments, it has been observed that the unique frequency is related to the large-scale circulation (LSC) in a helium gas cylindrical cell with $\Gamma=1$ [6–8], and its value is more or less the same as the circulation frequency of the large convective flow. A coupled-oscillator model was proposed to explain the observed phenomenon, in which the plume clusters from one plate are triggered by those from the opposite plate and the overall process will be self-sustained [9]. A prediction of the model is that the oscillation period is twice of the cell-crossing time of the clustered plumes. This has been verified by later direct velocity measurements [17,18,24]. All the above-mentioned models suggest that the thermal plumes and the thermal boundary layers play a dominant role in the generation of the oscillation.

In thermal convection, it has been found that, for the most part, the LSC has a preferred orientation in $\Gamma=1$ cylindrical cells and it oscillates azimuthally around this orientation [22,23,26,28,30]. Recently, several new dynamic processes—e.g., reorientation, cessation, and so on—have been observed in cylindrical cells [15,23,30]. Based on the phenomenon of horizontal oscillations of LSC [22], a new dynamical model has been proposed [26,28]. This model suggests that the horizontal oscillation of large-scale flow is the main source of the low-frequency oscillation in the system. Instead of being caused by periodic plume ejections from the boundary layers, this horizontal oscillation is intrinsic to the bulk dynamics. The periodical ejections of plumes may then be viewed as passive objects of the process.

The LSC dynamical picture can be simplified if large-scale reorientations or cessations are not considered; the horizontal oscillation of LSC will be analogous to a classical harmonic oscillator wandering around its origin. In this case, one may wonder whether the system geometry plays a role in the horizontal oscillations of the LSC. In most cases experiments and simulations have been performed mainly in a cylindrical cell of aspect ratio 1 in which axis symmetry holds and only one large-scale convective roll exists [6–10,14–25,28–30]. At low Ra, the linear stability analysis predicted that one asymmetric convection roll occupies the whole bulk regime when the cell provides an axis-symmetric boundary condition [31] and the convection roll could be

*sqzhou@phy.cuhk.edu.hk

aligned in any direction around the circle [32]. But in real systems there are inevitably imperfections, initial instabilities, and other external factors, which lead to the evolution of one stable branch, with all other branches being unstable [33]. In numerical simulations, a similar picture could be expected for the case of high-Ra convection [34].

In this paper, we report turbulent thermal convection experiments in a rectangular cell, in which the axis symmetry is absent. Local velocity and temperature measurements at various locations were made over varying values of Ra and at a fixed Pr. We focus on the oscillatory behavior of measured local velocity and temperature fields. The remaining sections of the paper are organized as follows. In Sec. II we describe the rectangular convection cell and the velocity and temperature measurements. In Sec. III, we present and discuss the experimental results. There we first show the autocorrelation functions and histograms of the velocity and temperature signals. We also discuss the spatial distribution of the velocity and temperature oscillations. We then present the Ra dependence of the periods of these oscillations. A brief summary is given in Sec. IV.

II. EXPERIMENT SETUP

The convection cell has a square vertical cross section, and its length, width, and height are $81\times20\times81$ (cm^3), as shown in Fig. 1(a). With this geometry, the axis symmetry does not exist and the large-scale flow is expected to be largely confined in the plane with the aspect ratio $\Gamma=1$. The working fluid was water. A detailed description of the apparatus can be found in Ref. [35]. Here the coordinates are defined as follows: the origin coincides with the cell center, its x axis points to the right, the z axis points upward, and the y axis points inward. We measured the velocity and temperature signals at positions marked by the solid lines in Fig. 1(b). The velocity was measured by laser Doppler anemometry (LDA), and the measurement volume was approximately 0.12 mm in diameter and 1.1 mm in length [16]. Along the line $(x,0,0)$, the two-dimensional velocity (v_y, v_z) was measured, and the velocity (v_x, v_z) was measured along the line $(0,0,z)$. At each position $\sim10^6$ or at least 5.2 h statistically independent samples were acquired. The temperature measurement apparatus was similar to that described in Ref. [36]. The local temperature was measured by using a thermistor about 300 μm in size. The thermistor served as one arm of an ac Wheatstone bridge driven sinusoidally at 1 kHz in frequency and 0.5 V in amplitude. The output of the bridge was first fed to a lock-in amplifier and then digitized by a dynamic signal analyzer at a sampling rate of 128 Hz; the recording time was 4.5 h to ensure good data statistics. Ra and Pr were kept at 8.9×10^{11} and 4.0, respectively, unless stated otherwise.

III. RESULTS AND DISCUSSION

A. Autocorrelation function and histogram

To test whether a low-frequency oscillation exists we analyze the autocorrelation function $C(t)=\langle\delta X(\tau)\delta X(\tau+t)\rangle$ of these measured signals. Here δX is the fluctuation of X normalized by its rms value, X can be v_x, v_y, v_z, and T, and $\langle\cdot\rangle$ denotes the time average. Examples of the autocorrelations of v_y, v_z, and T at (385 mm,0,0) near the sidewall are shown in Fig. 2(a). An oscillation can be found in v_y, whose intensity, represented by the magnitude of the second-order peak, is as strong as that observed in the vertical velocity measurement near the sidewall of cylindrical cells [16,20,21]. But the vertical velocity v_z here shows no oscillation from its autocorrelation function, which differs from that in the cylindrical cells [16,20,21]. The oscillation of the temperature signal is much weaker than that in the cylindrical cell [21], but the second-order peak can be well resolved from the background noise fluctuation. The oscillation periods obtained from v_y and T are denoted as t_v and t_T, respectively. When the measurement moves away from the sidewall to the region of the cell, as shown in Fig. 2(b) where the location is (240 mm,0,0), the velocity oscillation cannot be observed from both v_y and v_z components, whereas temperature oscillations can still be detected. In the measurement along the line $(0,0,z)$, two examples at $(0,0,-385$ mm) and

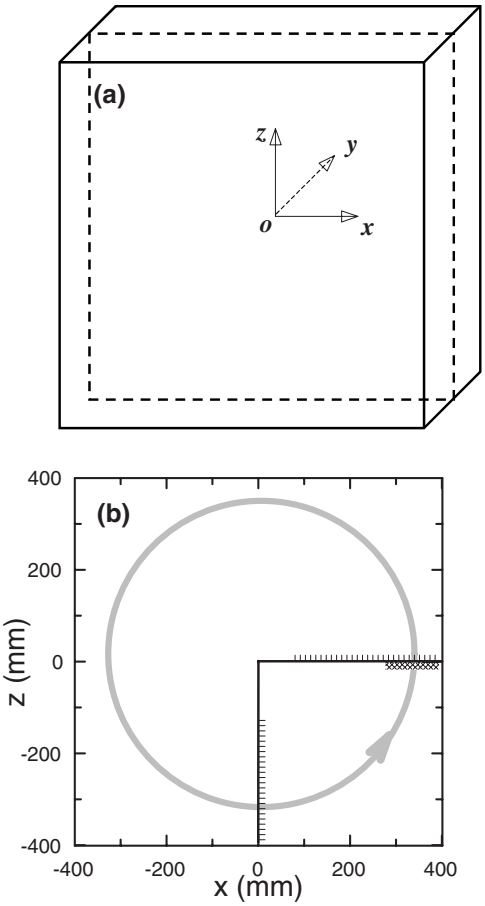

FIG. 1. (a) Schematic drawing of the convection cell and the coordinates for the experiment. (b) The x-z cross-section plane of the cell at $y=0$ [shown as the dashed plane in (a)]. Inside the plane, the large-scale flow is demonstrated as the gray circle. The measured positions are along the marked solid lines, and the positions where the oscillation can be found from temperature signal are indicated by the line combs, those from velocity by the line diamonds.

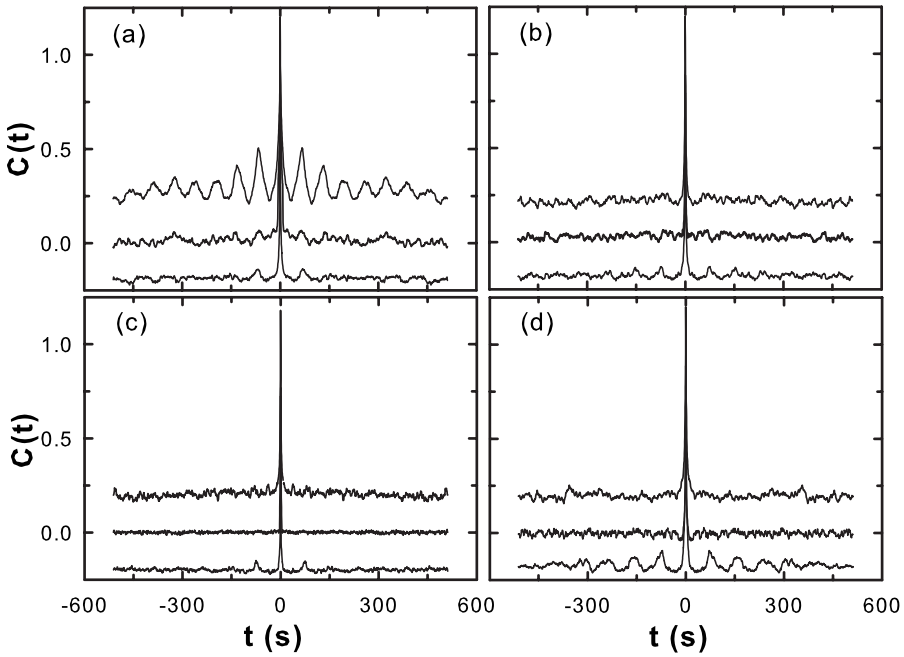

FIG. 2. (a) Top to bottom curves: autocorrelation functions of v_y (shifted up by 0.2), v_z, and temperature (shifted down by 0.2) at (385 mm,0,0). (b) Same as (a) but at (240 mm,0,0). (c) Top to bottom curves: autocorrelation functions of v_x (shifted up by 0.2), v_z, and temperature (shifted down by 0.2) at (0,0,−385 mm). (d) Same as (c) but at (0,0,−240 mm).

(0,0,−240 mm) are shown in Figs. 2(c) and 2(d), respectively, in which only temperature oscillation can be observed; the velocity one cannot be detected in either v_x or v_z component.

We now examine the histograms of these velocity signals; some examples are shown in Fig. 3. Along the line $(x,0,0)$, there are two peaks in the histogram of v_y at location (385 mm,0,0) [Fig. 3(a)], and it can be fitted with a two-

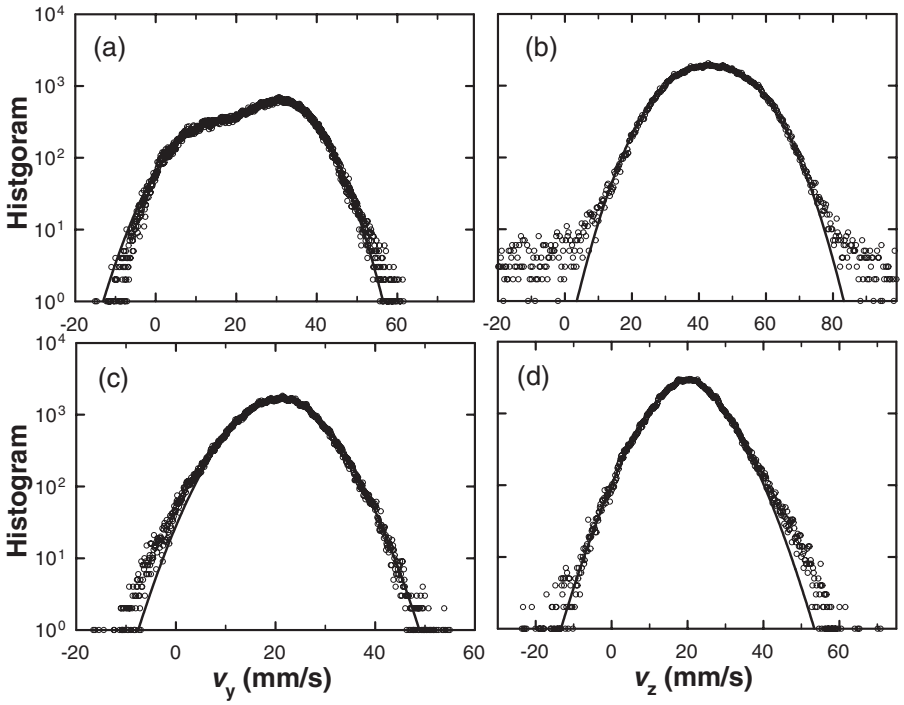

FIG. 3. Histograms of (a) v_y at (385 mm,0,0), (b) v_z at (385 mm,0,0), (c) v_y at (240 mm,0,0), and (d) v_z at (240 mm,0,0). Their fitting curves are plotted in solid lines from (a) two-peak Gaussian function, (b) one-peak Gaussian function, and (c) and (d) one-peak exponential power function.

peak Gaussian function. The distribution of v_y has two peaks which is consistent with the strong horizontal velocity oscillation shown in its autocorrelation function [Fig. 2(a)]. The histogram of v_z [Fig. 3(b)] exhibits a typical Gaussian-like distribution; it is also consistent with the behavior in its autocorrelation function [Fig. 2(a)]. At location (240 mm,0,0), both velocity components v_y and v_z have similar single-peaked histograms [Figs. 3(c) and 3(d)]. They can be fitted by a stretched exponential function $\left(\sim\exp\left[-\frac{(x-x_0)\beta}{b}\right]\right)$; here, the fitted β is 1.6±0.1. Note that the peak values of v_y are nonzero at both positions (385 mm,0,0) and (240 mm,0,0),which means the large-scale flow is not strictly rotating in the vertical x-z plane. In the previous particle image velocimetry (PIV) measurement, it has been observed that the large-scale flow along the diagonal direction is in the y-z plane at higher Ra [35], our result is consistent with the observation. We also examined the histograms for both the v_x and v_z velocity components along the line $(0,0,z)$ and find single-peaked Gaussian-like distributions for positions close to the bottom plate and stretched-exponential distribution for locations far away from the plate. Such results are consistent with the observations that no oscillation in their autocorrelation functions [Figs. 2(b)–2(d)].

It is a surprise that the oscillation in the velocity field cannot be observed in its vertical component v_z. A similar finding has also been reported in the PIV measurement of the present system [35], where no velocity oscillation has been seen in the large-scale circulation plane. Such an observation is different from that in the cylindrical cell and does not support the "plume model" explanations [3,9,14,17–20,24,29]. If the thermal plumes are ejected from the conducting plates in a periodical manner [19,20,29], the vertical velocity v_z should contain an oscillatory character because the thermal plumes are driven by the buoyancy force. The absence of this oscillation suggests that temperature and velocity oscillations may have different origins and be controlled by different mechanisms.

B. Spatial distribution

One can see that both temperature and velocity oscillations can be observed in the present system (although not at all positions). The positions where the oscillation can be found from T and v_y are marked in Fig. 1(b). The temperature oscillation can be detected in the range $x \in \{80\text{ mm}, 395\text{ mm}\}$ along the line $(x,0,0)$ and $z \in \{-130\text{ mm}, -387\text{ mm}\}$ along the line $(0,0,z)$. There is no temperature oscillation in the central region of the cell. We examine the data in the cylindrical cell of Ref. [37] and find the same result. However, in the cylindrical cell, it has been found that the temperature oscillation near the sidewall is much stronger than that near the bottom plate [19]. Here we cannot distinguish where the temperature oscillation is obviously stronger from the autocorrelations, as shown in Fig. 2.

From Fig. 1(b), we can see that velocity oscillation can only be detected in its component v_y near the sidewall ($x \in \{250\text{ mm}, 395\text{ mm}\}$). Correspondingly, at these positions two peaks have been observed in the histogram of v_y. The peak values of v_y in the histograms are shown in Fig. 4. The difference between the two peak values becomes smaller as the measuring position moves away from the sidewall to the central region and the two values merge into one at x around 250 mm, where the oscillation becomes undetectable in the velocity field, as illustrated in Fig. 1. Oscillations cannot be found at other measured positions, including v_y and v_z in the range $x \in \{0,250\text{ mm}\}$ along the line $(x,0,0)$ and v_x and v_z in the whole line $(0,0,z)$. The result is in sharp contrast to what is observed in the cylindrical cell [20,24]. In the cylindrical cell, oscillations could be found everywhere in the bulk regime from the horizontal velocity measurement and the oscillating intensity is stronger in the center than that in other positions [24]. Recently, oscillations have also been explored in a rectangular cell, where the horizontal cross section is square and the aspect ratio $\Gamma=4$ [27]. But the authors found that oscillations stem from the periodical switching between two corotating convective rolls. The oscillations observed in the present system should not share the same dynamic mechanism as that case because only one large-scale roll exists here [35].

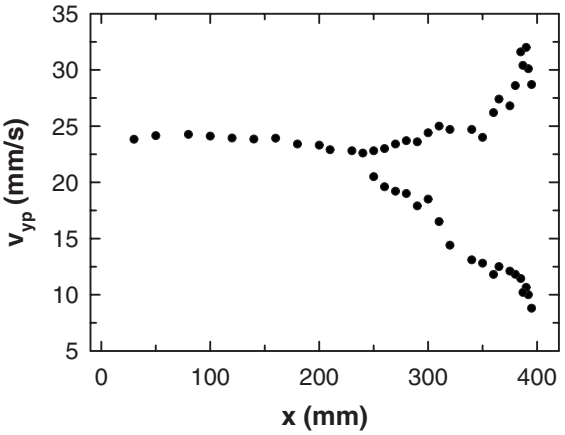

FIG. 4. The peak values of v_y as function of x when the measured position moves from the cell center to the sidewall.

Next, we discuss the position dependence of temperature (t_T) and velocity (t_v) oscillation periods, respectively. As shown in Fig. 5, we can see that within experimental uncertainty the temperature oscillation period (t_T) may be regarded as a constant, $t_T=74\pm2$ s, for all measured positions on both the vertical and horizontal scans. The fact that temperature oscillations can be observed in most parts of the measured locations with the concordant oscillation period implies that it is a global characteristic of the convective flow and the oscillation period can be a typical time scale to describe the flow system. Oscillations of the velocity field can only be observed in a rather narrow region close to the sidewall, inside which region the turbulent intensity was found to be the strongest in the system [35]. The velocity oscillation period (t_v) also remains more or less constant, $t_v=65\pm2$ s, for all measured positions. Note that t_v is about 14% less than t_T; such a difference between the two oscillation periods is beyond the experimental uncertainties for the respective measurements.

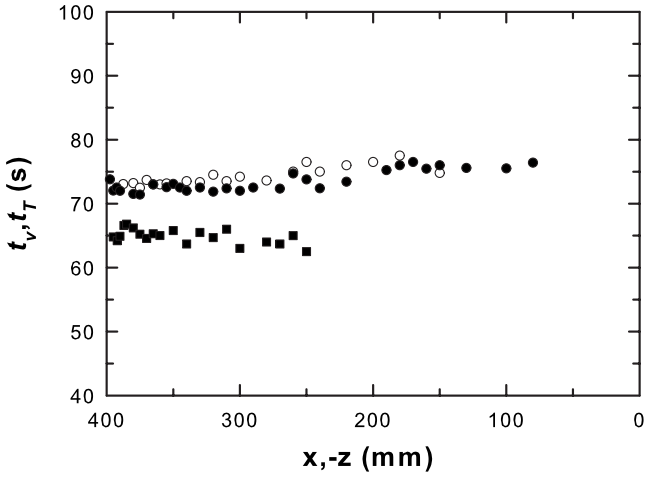

FIG. 5. The measured oscillation periods from the velocity v_y along the line $(x,0,0)$ (solid squares) and temperature signals along the lines $(x,0,0)$ (open circles) and $(0,0,z)$ (solid circles).

C. Ra dependence

Keeping constant Pr=4.0, we also measured the oscillation periods (t_T and t_v) of temperature and velocity fields over the range of Ra from 2×10^{10} to 8.9×10^{11}. In order to compare to previous results in the literature [10,15,19,20,22,35], $t_{T(v)}$ is normalized in the form of the Péclet number $\left(\mathrm{Pe}_{T(v)} \equiv \frac{UL}{\kappa} = \frac{4L^2}{t_{T(v)}\kappa}\right)$; here, the subscript of Pe denotes that it is obtained from either the temperature or velocity, and the typical velocity U is represented by $\frac{4L}{t_{T(v)}}$. As shown in Fig. 6, we can see that Pe_T and Pe_v have comparable magnitude, but their difference can be well discerned. The Ra dependence of Pe_T can be fitted with $0.55\mathrm{Ra}^{0.47}$. The exponent agrees excellently with the temperature oscillation measurements in low-temperature helium gas [15], mercury [10], and water [19] of a cylindrical cell; the different prefactors are perhaps due to the fluids of different Pr. Moreover, the scaling is consistent with that of the angular oscillations of the horizontal thermal plume motion above the bottom plate in a cylindrical cell [22]. This result confirms that the temperature oscillation has global and universal character in thermal convection, and this result also implies that the temperature oscillation period (t_T) is contributed from the flow motions of thermal structures and independent of system geometry. We also notice that some experiments have reported different scalings for temperature oscillation periods (t_T) in the cylindrical cell [8,12,25]. One possible explanation is that the path length of the circulation affects the scaling of the oscillation period [25].

In the cylindrical cell, it was reported that the velocity oscillation follows $0.167\mathrm{Ra}^{0.47}$ and it is driven by the same mechanism as that of temperature [19,20]. That is, the velocity and temperature oscillations are generated by the alternating emission of thermal plumes between the upper and lower thermal boundary layers [20]. Moreover, it was found that both temperature and velocity oscillation periods are coincident with the rotational period of large-scale circulation [17,18,20]. In the present system, the Ra dependence of Pe_v is fitted as $0.29\mathrm{Ra}^{0.50}$. Considering its previous PIV measurement [35], the rotation rate of large-scale circulation has been obtained and the Pe could be fitted with the formula $0.318\mathrm{Ra}^{0.496}$, which is replotted in Fig. 6. We can see that the Péclet number Pe_v agrees with this fitting line very well, but the temperature Pe_T does not. These results suggest that the velocity oscillation period is consistent with the rotational period of the large-scale flow in both cylindrical and rectangular cells, and both of them could be affected by the system geometry. Based on the results that temperature and velocity oscillations have different responses to the system geometry, it may be proposed that the two oscillations reflect different aspects of the thermal convective flow even though they are related to each other.

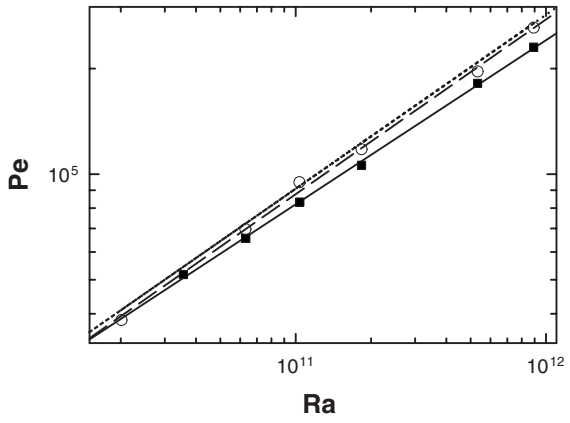

FIG. 6. The Ra dependence of the Péclet number. Pe_v from the velocity oscillation (open circles) and its fitting $0.29\mathrm{Ra}^{0.50}$ is plotted as dash line; Pe_T from the temperature oscillation (solid squares) and its fitting $0.55\mathrm{Ra}^{0.47}$ is plotted as solid line; Péclet number obtained from the rotational rate in the PIV measurement [35] is plotted here as dotted line.

IV. CONCLUSION

In this work, both temperature and velocity oscillations can be found in the rectangular cell, where only one large-scale convection roll exists. At fixed Ra (8.9×10^{11}), it is found that temperature oscillations can be observed in most locations in which measurements were made, and they give a position-independent oscillation period $t_T=74\pm2$ s. For measurements made with different Ra, the normalized oscillation period Pe_T is found to scale as $0.55\mathrm{Ra}^{0.47}$, which is the same as that found in cylindrical cells [10,15,19,20]. This scaling is also the same as that obtained from the horizontal motions of thermal structures (plumes) [22]. This result suggests that temperature oscillation is a global and universal characteristic of turbulent thermal convection and its statistical behaviors may be related to the flow motions of thermal structures and are independent of system geometry.

It is a surprise that the oscillation in the velocity field cannot be seen in its vertical component v_z near the sidewall. If the thermal bursts are erupted in a periodical way, it should be detected by the vertical velocity because the thermal bursts are driven vertically under the buoyancy force. How-

ever, velocity oscillation can only be observed in its horizontal component (v_y) at positions close to the sidewall, where its histogram exhibits two peaks. The normalized velocity oscillation period Pe_v shows an Ra dependence of $\mathrm{Ra}^{0.50}$ and it collapses very well on that obtained from the rotation rate of convective flow [35]. This is different from the observation in the cylindrical cell [20], where it was reported that the periods for both the velocity and temperature oscillations and the rotational period of the convective flow follow the same scaling [17,20]. This comparison suggests that the velocity oscillation period is consistent with that obtained from the rotation rate of the large-scale flow, and both of them could be affected by the system geometry.

ACKNOWLEDGMENTS

We would like to thank G. Ahlers and H.-D. Xi for illuminating discussions. K.-Q.X. was supported by Hong Kong RGC Grant No. 403705. S.-Q.Z. was supported by CUHK direct Grant No. 2060309 and United College research Grant No. CA11096.

[1] B. W. Atkinson and J. W. Zhang, Rev. Geophys. **34**, 403 (1996).
[2] W. V. R. Malkus, Proc. R. Soc. London, Ser. A **225**, 185 (1954).
[3] L. N. Howard, in *Proceedings of the 11th Congress of Applied Mechanics*, edited by H. Grtler (Springer-Verlag, Berlin, 1964), p. 1109.
[4] E. B. Siggia, Annu. Rev. Fluid Mech. **26**, 136 (1994).
[5] R. Krishnamurti and L. N. Howard, Proc. Natl. Acad. Sci. U.S.A. **78**, 1981 (1981).
[6] F. Heslot, B. Castaing, and A. Libchaber, Phys. Rev. A **36**, 5870 (1987).
[7] M. Sano, X.-Z. Wu, and A. Libchaber, Phys. Rev. A **40**, 6421 (1989).
[8] B. Castaing, G. Gunaratne, F. Heslot, L. Kadanoff, A. Libchaber, S. Thomae, X.-Z. Wu, S. Zaleski, and G.-M. Zanetti, J. Fluid Mech. **204**, 1 (1989).
[9] E. Villermaux, Phys. Rev. Lett. **75**, 4618 (1995).
[10] T. Takeshita, T. Segawa, J. A. Glazier, and M. Sano, Phys. Rev. Lett. **76**, 1465 (1996).
[11] S. Ciliberto, S. Cioni, and C. Laroche, Phys. Rev. E **54**, R5901 (1996).
[12] S. Cioni, S. Ciliberto, and J. Sommeria, J. Fluid Mech. **335**, 111 (1997).
[13] S. Ashkenazi and V. Steinberg, Phys. Rev. Lett. **83**, 3641 (1999).
[14] R. Krishnamurti, Sadhana: Proc., Indian Acad. Sci. **23**, 605 (1999).
[15] J. J. Niemela, L. Skrbek, K. R. Sreenivasan, and R. J. Donnelly, J. Fluid Mech. **449**, 169 (2001).
[16] X.-D. Shang and K.-Q. Xia, Phys. Rev. E **64**, 065301(R) (2001).
[17] X.-L. Qiu and P. Tong, Phys. Rev. Lett. **87**, 094501 (2001).
[18] X.-L. Qiu and P. Tong, Phys. Rev. E **64**, 036304 (2001).
[19] X.-L. Qiu and P. Tong, Phys. Rev. E **66**, 026308 (2002).
[20] X.-L. Qiu, X.-D. Shang, P. Tong, and K.-Q. Xia, Phys. Fluids **16**, 412 (2004).
[21] X.-D. Shang, X.-L. Qiu, P. Tong, and K.-Q. Xia, Phys. Rev. E **70**, 026308 (2004).
[22] D. Funfschilling and G. Ahlers, Phys. Rev. Lett. **92**, 194502 (2004).
[23] E. Brown and G. Ahlers, J. Fluid Mech. **568**, 351 (2006).
[24] C. Sun, K.-Q. Xia, and P. Tong, Phys. Rev. E **72**, 026302 (2005).
[25] C. Sun and K.-Q. Xia, Phys. Rev. E **72**, 067302 (2005).
[26] C. Resagk, R. du Puits, A. Thess, F. V. Dolzhansky, S. Grossmann, F. F. Arauio, and D. Lohse, Phys. Fluids **18**, 095105 (2006).
[27] J. Verdoold, M. J. Tummers, and K. Hanjalic, Phys. Rev. E **73**, 056304 (2006).
[28] R. du Puits, C. Resagk, and A. Thess, Phys. Rev. E **75**, 016302 (2007).
[29] H.-D. Xi, S. Lam, and K.-Q. Xia, J. Fluid Mech. **503**, 47 (2004).
[30] H.-D. Xi, Q. Zhou, and K.-Q. Xia, Phys. Rev. E **73**, 056312 (2006).
[31] G. S. Charlson and R. L. Sani, Int. J. Heat Mass Transfer **14**, 2157 (1971).
[32] M. Golubitsky and D. Schaeffer, Proc. Symp. Pure Math **40**, 499 (1983).
[33] G. Neumann, J. Fluid Mech. **214**, 559 (1990).
[34] R. Verzicco and R. Camussi, Phys. Fluids **9**, 1287 (1997).
[35] K.-Q. Xia, C. Sun, and S.-Q. Zhou, Phys. Rev. E **68**, 066303 (2003).
[36] S.-Q. Zhou and K.-Q. Xia, Phys. Rev. E **63**, 046308 (2001).
[37] S.-Q. Zhou and K.-Q. Xia, Phys. Rev. Lett. **87**, 064501 (2001).